

# Experimental Studies and Numerical Analysis of the Inflation and Interaction of Vascular Balloon Catheter-Stent Systems

DIMITRIOS E. KIOUSIS,<sup>1</sup> ALEXANDER R. WULFF,<sup>2</sup> and GERHARD A. HOLZAPFEL<sup>1,2</sup>

<sup>1</sup>Institute of Biomechanics, Center of Biomedical Engineering, Graz University of Technology, Kronesgasse 5-I, 8010 Graz, Austria; and <sup>2</sup>Department of Solid Mechanics, School of Engineering Sciences, Royal Institute of Technology (KTH), Stockholm, Sweden

(Received 29 October 2007; accepted 12 June 2008; published online 2 December 2008)

**Abstract**—Balloon angioplasty with stenting is a well-established interventional procedure to treat stenotic arteries. Despite recent advances such as drug eluting stents, clinical studies suggest that stent design is linked to vascular injury. Additionally, dilation of the medical devices may trigger pathological responses such as growth and migration of vascular smooth cells, and may be a potent stimulus for neointimal hyperplasia. The purpose of this study is to experimentally investigate the mechanical characteristics of the transient expansion of six commercially available balloon-expandable stent systems, and to develop a robust finite element model based on the obtained experimental results. To reproduce the inflation of stent systems as in clinical practice, a pneumatic–hydraulic experimental setup is built, able to record loads and deformations. Characteristic pressure–diameter diagrams for the balloon-expandable stents and the detached balloons are experimentally obtained. Additionally, typical measures such as the burst opening pressure, the maximum dog-boning and foreshortening, and the elastic recoil are determined. The adopted constitutive models account for elastoplastic deformation of the stent, and for the nonlinear and anisotropic behavior of the balloon. The employed contact algorithm, based on a  $C^2$ -continuous surface parametrization, efficiently simulates the interaction of the balloon and stent. The computational model is able to successfully capture the experimentally observed deformation mechanisms. Overall, the numerical results are in satisfactory agreement with experimental data.

**Keywords**—Stent, Balloon catheter, Expansion, Constitutive modeling, Contact, Experiment, Finite element method.

## INTRODUCTION

The latest medical statistics reveal that one out of three Americans has one or more types of cardiovascular disease (CVD).<sup>46</sup> Similarly, CVDs cause nearly half of all deaths in Europe.<sup>1</sup> CVDs are mostly related

to common arterial disorders such as atherosclerosis, which, due to the deposition of fatty substances on arterial walls, reduce the lumen area and decrease the blood flow and the transport of oxygen and nutrients to the organs. An effective and widely used remedy to treat occluded arteries is balloon angioplasty with stenting. The minimally invasive nature of this procedure and its remarkably high initial success rate<sup>21,47</sup> have made balloon angioplasty an attractive therapeutic method. In addition, recently introduced technology to release drugs locally via polymeric-coated stents has proven remarkably safe and effective in preventing neointima formation, and has reduced short-term rates of restenosis.<sup>8,18,26,38,50</sup>

Nevertheless, the overexpansion of the lesions during angioplasty still induces mechanical injury, which triggers pathological responses such as neointimal hyperplasia.<sup>14,17</sup> These responses are key factor in in-stent restenosis,<sup>6,19,30,39</sup> the most important long-term limitation of stent implantation. It is important to note that the mechanical injury to the vessels is not eliminated by drug-eluting stents.

Balloon angioplasty and stenting is a mechanical solution to a clinical problem. Hence, one may claim that the imposed vascular injury and the resulting restenosis depend on the stent design (structure and material) and the deployment technique, and consequently on the way the medical devices interact with the lesion. Indeed, several clinical studies show the effect of device-dependent factors such as the stent design<sup>29,34,45,51</sup> and deployment technique<sup>20,29</sup> on tissue proliferation and restenosis. In addition, the review article by Morton *et al.*<sup>37</sup> summarizes a series of trials and comparative studies which strongly demonstrate that arterial trauma is a function of stent structure and dimensions, i.e., mechanics.

The delicate balance between maximum final stent diameter and minimal arterial trauma, and the elimination of restenosis, has motivated intensive research

Address correspondence to Gerhard A. Holzapfel, Institute of Biomechanics, Center of Biomedical Engineering, Graz University of Technology, Kronesgasse 5-I, 8010 Graz, Austria. Electronic mail: holzapfel@tugraz.at

efforts in the bioengineering community. A majority of studies focus on understanding the mechanical behavior and the optimal clinical function of the balloon-stent system. A few experimental studies<sup>4,12,41,44</sup> provide comparisons of different stents based on physical and mechanical properties such as hoop strength, structural integrity, recoil, and flexibility. Two other papers<sup>5,40</sup> deal with the dilation behavior of balloon-expandable coronary stents and the characteristic nonlinear behavior of the stenting system under internal pressure.

In addition to experimental investigations a large number of finite element approaches exist. The majority of published numerical models focus on the stent's deformation characteristics during expansion,<sup>13,16,54</sup> and discuss the localized stress regions in the stent structure.<sup>7,11</sup> Several studies,<sup>10,35</sup> discuss particular features of the behavior of stents such as dog-boning and foreshortening. The documented results are of particular interest as they may be linked to neointima formation. For example, the nonuniform expansion (dog-boning) of the stent is one cause for the injured areas around the stent edges, and excessive axial contraction of the stent (foreshortening) affects the device positioning and injures the thin endothelial layer.

To the authors' knowledge, very few numerical studies aim to further validate their results with experimental data. The paper by Brauer *et al.*<sup>5</sup> combines experimental data with numerical analysis, though the agreement is rather poor. The computational study by Migliavacca *et al.*<sup>36</sup> analyzes the radial expansion and the recoil of coronary stents. The areas of plastic stent deformation are matched to experimental data obtained from scanning electron microscopy. In the numerical model however, the balloon is not considered. A promising study by De Beule *et al.*<sup>9</sup> documents a numerical model for the dilation of a coronary balloon-stent system, wherein the actual folded shape of the balloon and the initial crimping of the stent on the catheter are considered. For the balloon, an elastic material model is used. The authors claim strong correlation with the manufacturer's data, and identify that the crimping procedure prior to the stent's expansion has a minor influence on the overall stent behavior. The detailed investigation by Wang *et al.*<sup>53</sup> focuses on the transitory nonuniform expansion (dog-boning) and foreshortening of six stent models. The balloon is considered to be cylindrical, and it is modeled as an isotropic, linear elastic material. The results indicate that dog-boning depends on the geometry of the stent's distal cells and on the overlength of the balloon. The authors also formulate a semi-quantitative comparison between the measurements and simulation; a good match is shown.

The above-mentioned studies provide a useful benchmark for the identification and characterization of the balloon-stent expansion characteristics. However, there is still a need for more advanced and efficient models that incorporate the highly nonlinear behavior of the individual components of the system, and the complexity of their contact interaction. Additionally, the validation of these models with pertinent experimental data is crucial.

The present work is a further step in this direction. The authors start by seeking an understanding of the complex, nonlinear transient inflation of different, commercially available balloon-expandable stent systems on an experimental basis. Then, based on the obtained data, they present a finite element model that is able to reproduce the characteristic inflation mechanism. To this end, cooperations with the Swedish subsidiaries of three industry-leading stent manufacturers (Boston Scientific, Cordis, and Medtronic) are established and six stents, premounted on balloon catheters, are acquired. As part of the experimental investigations, a pneumatic-hydraulic system is built and the deformations of the catheter-stent systems are recorded. Furthermore, mechanical behaviors such as dog-boning, foreshortening and recoil are analyzed. Next, a numerical framework is developed which considers the nonlinearity and anisotropy of the balloon and the elastoplastic deformation of the stent. Three-dimensional interaction between the catheter and the stent is modeled by means of  $C^2$ -continuous surfaces. For one of the stents, detailed numerical results of the balloon-stent dilation modeling are presented in terms of pressure-deformation diagrams.

## EXPERIMENTAL STUDY

The goal is to investigate the deformation mechanisms (change in diameter and length) of the six sample balloon-expandable stent systems under operational internal pressure that range between 0 and 12 bar (the burst pressure was approximately 15 bar). Inflation tests are examined for dog-boning and foreshortening. Another goal is to better understand the mechanical behavior of angioplasty balloons under internal pressure loading. For this purpose, the balloon catheters are detached from the catheter-stent system, and characteristic deformations are measured. The experimental data will assist in subsequent numerical modeling.

We provide details of the stent products under investigation and describe the experimental setup and procedure of the balloon catheter-stent inflation. The deformation mechanisms are presented and a comparison between the performance of the different stents

and balloon catheters is provided. Finally, we describe the experimental approach to test angioplasty balloons.

### *Investigated Balloon Catheter-Stent Systems*

In cooperation with three stent manufactures, Boston Scientific, Cordis, and Medtronic, six balloon catheter-stent systems were acquired (see Table 1). These stents are designed to target peripheral vascular lesions (located, for example, in the aorta or in the renal or femoral arteries) or the bile duct. Each manufacturer supplied two stent types, premounted on the delivery system (balloon catheter, guide wire, introducer sheath). Each set of two stents had a similar geometric shape but differed in dimensions. Figure 1 shows photographs of one stent product from each manufacturer in the fully expanded configuration (for clarity). The images were obtained by use of a CCD camera with a magnifying lens.

As can be seen in Fig. 1, geometric similarities are present among the three stents, for example, the sinusoidal strut structure. In all stents, three main building blocks are present: *unit*, *segment*, and *link*. A segment consists of several units connected circumferentially, while the axially positioned segments are attached by links, leading to the overall stent structure. The three manufacturers' stents have segments of similar shape but different links. More specifically, the stents from Boston Scientific and Medtronic have straight-shaped links of different lengths, while the stents from Cordis have s-shaped links. In addition, the Express Vascular LD and the Express Vascular SD have interchanging segments of different lengths with different numbers of units. This is not the case for the other four stent products. All the stents are made of surgical stainless steel 316L, except the Racer stent, which is made of a cobalt alloy (MP35N).

### *Experimental Setup and Procedure*

The experimental setup accommodates two tasks: (i) the application of a pressure load inside the balloon causing a dilation of the balloon expandable stent, and

(ii) the measurement of the load and the related deformation of the catheter-stent system. A schematic representation of the setup is depicted in Fig. 2. It is a simple, low cost pneumatic-hydraulic system, enhanced by two computer units and a camera.

The first step of the experimental process is concerned with the fixation of the catheter-stent system which is clamped at locations far away from its upper and lower boundaries. This allowed free expansion of the balloon in all three directions (radial, axial, and circumferential). In addition, the removal of the air from the inflation tube and the balloon catheter is carried out. Sterile water is used as inflation medium and therefore, all air must initially be evacuated from the system. This preparatory task is here performed as in clinical practice. In short, a stopcock along with a syringe are attached to the catheter's inflation port. While the stopcock is open, negative pressure is applied through the syringe. When total vacuum is achieved in the inflation lumen and balloon, the stopcock is closed and the syringe is removed. The flow of the sterile water into the balloon then takes place and the inflation of the balloon-stent system is initiated.

To gradually increase the pressure of the water, a compressed gas accumulator is used. One side of the accumulator is connected to a tube containing pressurized nitrogen, while the other chamber of the accumulator contains the hydraulic fluid (sterile water). The two media are separated by an elastic diaphragm. The progressive opening of the regulating vent connected to the gas tube leads to the gradational increase of the water's pressure, constantly measured by a pressure transducer located next to the catheter inflation port. The recording of the transducer is considered equal to the inner balloon pressure, by regarding the hydraulic losses negligible, and is subsequently labeled as  $p_b$ . The computer unit PC 2 records the input from the pressure transducer (the inflation load) at one second intervals, and simultaneously sends a signal to the computer unit PC 1. Simultaneously, PC 1 triggers a CCD camera equipped with a magnifying lens which takes a photograph of the catheter-stent system under dilation. Three examples of the acquired photographs are given in Fig. 3,

**TABLE 1. Product details of six balloon-expandable stents.**

| Company           | Product             | Material     | Stent diameter (mm) | Stent length (mm) |
|-------------------|---------------------|--------------|---------------------|-------------------|
| Boston Scientific | Express Vascular LD | 316L SS      | 9                   | 37                |
| Boston Scientific | Express Vascular SD | 316L SS      | 7                   | 15                |
| Cordis            | Palmaz Genesis      | 316L SS      | 7                   | 12                |
| Cordis            | Genesis Opti Pro    | 316L SS      | 7                   | 59                |
| Medtronic         | Bridge Assurant     | 316L SS      | 6                   | 20                |
| Medtronic         | Racer               | Cobalt alloy | 4                   | 18                |

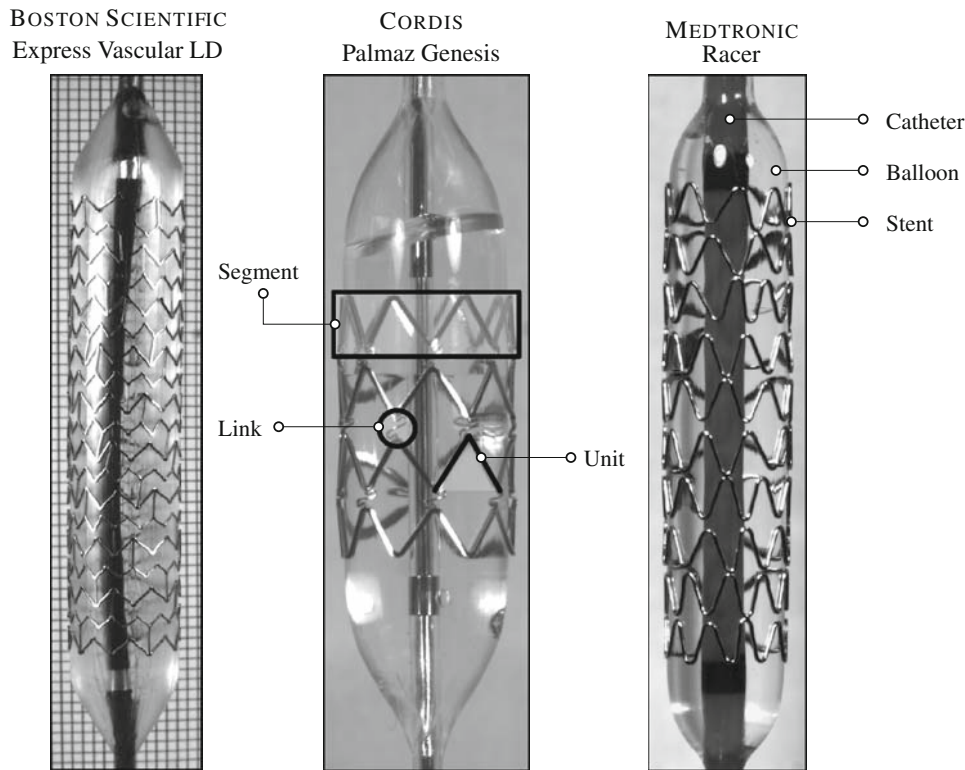


**FIGURE 1.** Fully inflated configuration of three balloon catheter-stent systems obtained from Boston Scientific, Cordis, and Medtronic. The parts of the systems (catheter, balloon, and stent) and the basic components of the stents (unit, segment, and link) are pointed out.

where the deformed configurations of the balloon-stent system at different inner balloon pressures are shown. Image analysis software (Scion Imaging) is employed for a detailed analysis of these data. Information such as the stent's diameter (at different positions, for example, at distal and central segments) and the total length at a specific pressure load is extracted.

### Experimental Results

The characteristic pressure–diameter ( $p$ – $D$ ) diagrams (i.e., the change of the stent's diameter with applied pressure load), can be determined for each stent by analyzing the obtained image data. The  $p$ – $D$  diagrams are a direct and comprehensive source of information concerning the deformation characteristics of the balloon catheter-stent systems. In addition, the diagrams provide an assessment of the different stent products with respect to their mechanical behavior. Figure 4 focuses on the Express Vascular LD balloon-stent system. In particular, Fig. 4(I) shows the gradual change of the inner balloon pressure  $p_b$  over time  $t$ , while Fig. 4(II) shows the change of the central diameter  $D_{st,c}$  over  $p_b$  (the  $D_{st,c}$ -measure is indicated in Fig. 3).

The diagrams of Fig. 4 indicate that the dilation of the Express Vascular LD balloon-stent system can be basically divided into four phases. Initially, as the pressure load starts to act on the inner side of the balloon catheter, the balloon fits closely to the stent. During this phase, ( $\textcircled{a} \rightarrow \textcircled{b}$ ) the stent deforms elastically and its central diameter  $D_{st,c}$  changes only slightly. This is not the case for the distal segments of the stent, where larger deformation is noted at the edges of the stent for the same pressure level ( $0 \leq p_b \lesssim 3$  bar). This behavior, called dog-boning (or bone effect), is due to a higher compliance at the ends of the stent structure, and is clearly visible in Fig. 3. According to Migliavacca *et al.*<sup>35</sup> dog-boning is defined as the ratio

$$DB = \frac{D_{st,d} - D_{st,c}}{D_{st,d}} \quad (1)$$

where the  $D_{st,d}$  is the diameter of the distal segment indicated in Fig. 3.

When the load reaches a specific limit, say  $p_b^*$  (for the Express LD,  $p_b^* = 2.90$  bar, see Fig. 4(II)), the stent starts to expand significantly (phase  $\textcircled{b} \rightarrow \textcircled{c}$ ), and the stent approaches its nominal diameter in a few seconds. The plateau of Fig. 4(II) shows this deformation

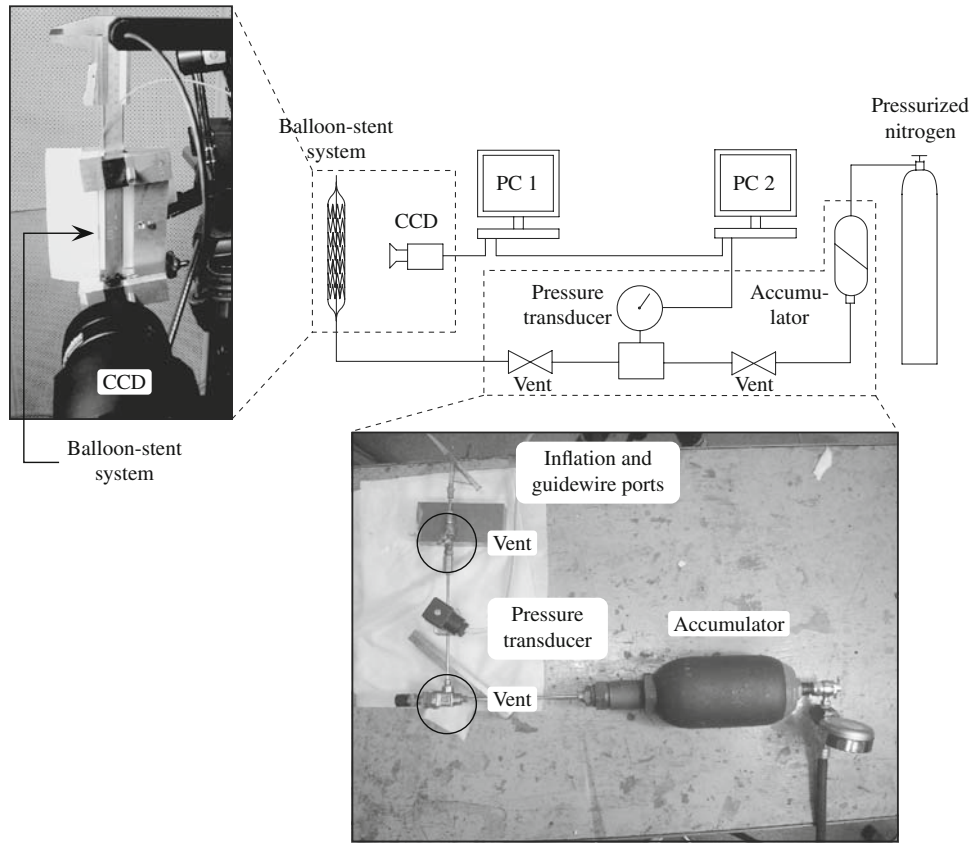


**FIGURE 2.** Schematic representation of the experimental setup used for the inflation of the balloon-expandable stents and for the recording of the load and deformation. The two photographs show various components of the setup.

mechanism. The main cause of this rapid expansion, referred to as burst opening, is the initiation of plastic deformation in some stent areas. The slight pressure drop during this phase is a consequence of the burst opening. As expected, when the diameter of the stent increases, then the volume increases causing a pressure drop. Subsequently, a new phase of deformation takes place (© → Ⓓ), wherein the balloon-expandable stent system stiffens significantly in the circumferential direction. A high pressure increase is recorded against a low stent dilation rate. The main cause of this stiffening behavior is plastic deformation of the stent and, most important, the deformation characteristics of the balloon catheter (as discussed later in the manuscript). Finally, the load is gradually removed (phase Ⓓ → Ⓔ) and the pressure is reduced to  $p_b = 0$  bar. The final diameter of the stent is smaller than its diameter at maximum pressure. This reduction in size is a result of the stent's elastoplastic deformation and is referred to as *recoil*. The central radial recoil  $RE_c^{rad}$  may be given by the relationship

$$RE_c^{rad} = \frac{D_{st,c}^{p_b^{max}} - D_{st,c}^{p_b^0}}{D_{st,c}^{p_b^{max}}}, \quad (2)$$

with  $D_{st,c}^{p_b^{max}}$  indicating the diameter of the stent's central segment at maximum pressure and  $D_{st,c}^{p_b^0}$  is the same diameter after deflation of the balloon. In the case of the Express LD stent, the recoil is approximately 1.5%, and therefore, not readily apparent in Fig. 4(II).

The mechanical responses of the other five stent products, as can be seen in Fig. 5, are qualitatively similar to that of the described Express LD system. In particular, Fig. 5 illustrates the respective changes in the central and distal diameters during the inflation of the six balloon-expandable stent systems. In all cases, the first three deformation phases (Ⓐ → Ⓑ → Ⓒ → Ⓓ) are visible. However, in each balloon-stent system a different burst opening pressure is recorded along with a different dilated diameter. A comparison between the distal and central segment clearly evinces the dog-boning effect, indicated by the faster expansion of the stent's edges. More specifically, at the distal segment, in all the cases, the burst opening pressure is approximately half the burst opening pressure of the central segment. A further difference between the central and the distal segment responses concerns the slight pressure drop during the burst opening. In the distal segments, the pressure decreases only just before the

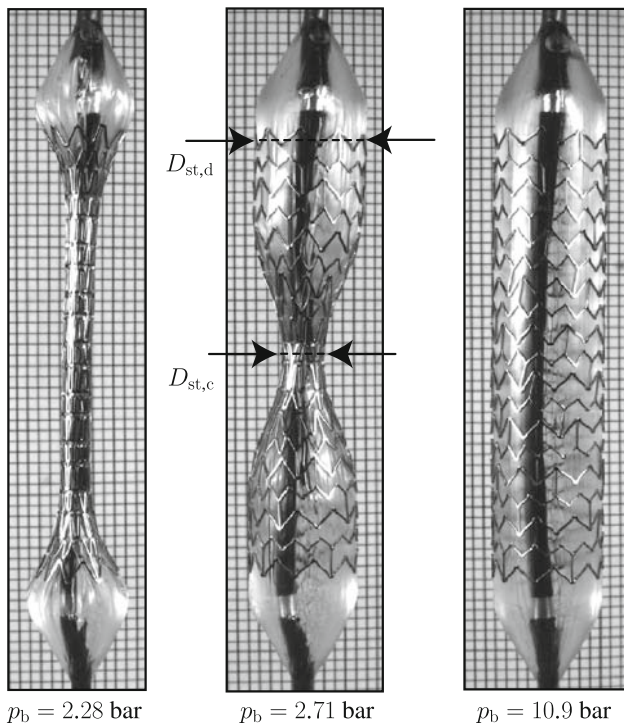


**FIGURE 3.** Three photographs taken during the inflation of an Express Vascular LD balloon-stent system. The deformed configurations of the balloon-catheter and the stent at three different inner balloon pressures  $p_b$  are displayed. From these images, and by means of image analysis software, the distal diameter  $D_{st,d}$  and the central diameter  $D_{st,c}$  of the stent were measured in addition to the total length. The dog-boning effect during the inflation of the balloon-expandable stent is clearly visible.

stiffening phase, while in the central segment it occurs during its (large) deformation. Note that other studies focusing on coronary stents<sup>5,53</sup> present similar  $p$ - $D$  curves to the ones depicted in the left diagrams of Fig. 5 (for reasons of clarity the unloading paths are not shown).

As was stated in the “Introduction” section, two important characteristic mechanisms of stent expansion are dog-boning and foreshortening. Dog-boning is observed in all investigated stents. Based on an Express LD stent, Fig. 6(I) shows the typical change of the dog-boning DB, according to Eq. (1), as a function of the inner balloon pressure  $p_b$ . The effect becomes clear at a pressure close to the burst opening pressure of the distal segments. When the balloon pressure reaches the value  $p_b^* \approx 3$  bar (central segment burst opening load) the stent approaches an approximately cylindrical shape and the dog-boning diminishes. At higher pressure loads and after deflation of the balloon catheter, the dog-boning decreases to zero.

The foreshortening mechanism describes the axial contraction of the stent under dilation. Foreshortening may be defined as<sup>35</sup>

$$FS = \frac{L_{st,defo} - L_{st,unde}}{L_{st,defo}}, \quad (3)$$

where  $L_{st,defo}$  and  $L_{st,unde}$  denote the deformed and the undeformed lengths of the stent, respectively. For the case of the Express LD stent, the change of foreshortening FS over inner balloon pressure  $p_b$  is depicted in

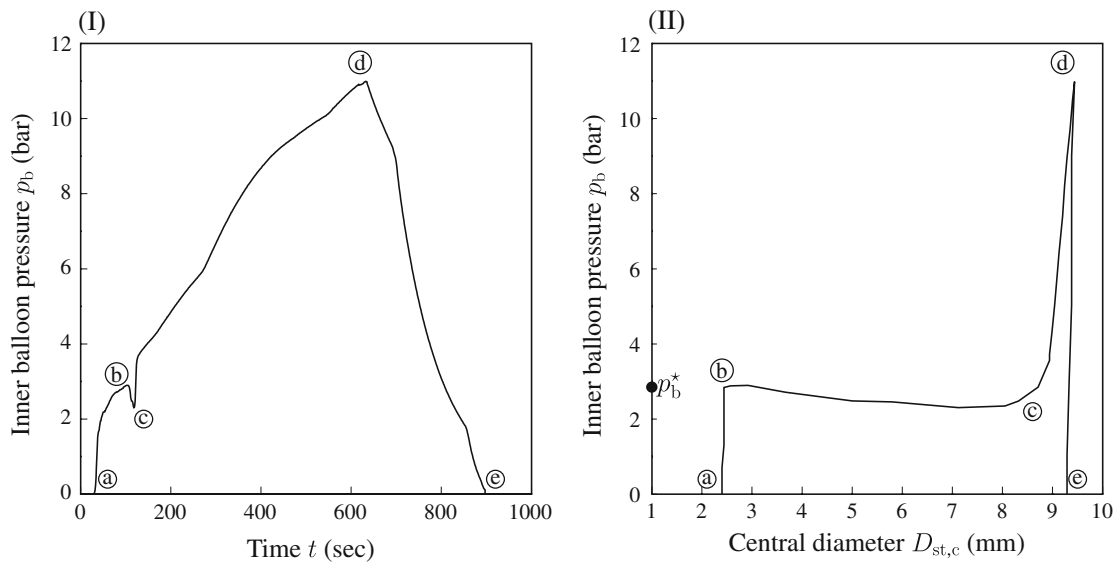


**FIGURE 4.** Change of the inner balloon pressure  $p_b$  over time  $t$  during inflation and deflation of an Express LD balloon-stent system (I). Change of the central diameter  $D_{st,c}$  of the stent over  $p_b$  (II). The deformation mechanism of balloon expandable stents is divided into four stages:  $\textcircled{a} \rightarrow \textcircled{b}$ , balloon fitting and elastic stent deformation;  $\textcircled{b} \rightarrow \textcircled{c}$ , burst opening accompanied with a large dilation rate;  $\textcircled{c} \rightarrow \textcircled{d}$ , circumferential stiffening;  $\textcircled{d} \rightarrow \textcircled{e}$ , load removal and (elastic) recoil.

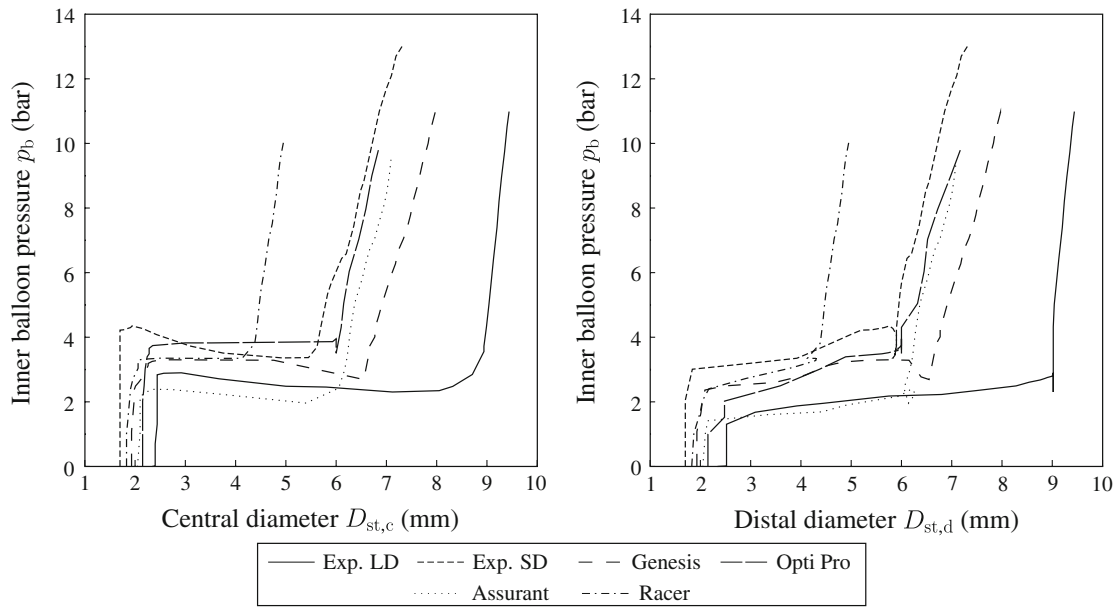


**FIGURE 5.** Change of the inner balloon pressure  $p_b$  vs. the central diameter  $D_{st,c}$  and the distal diameter  $D_{st,d}$  for six balloon-expandable stent systems (compare with Table 1). Similar deformation characteristics are identified for all the stent investigated products (three phase expansion), but also noticeable differences, for example, different burst opening loads and final diameters.

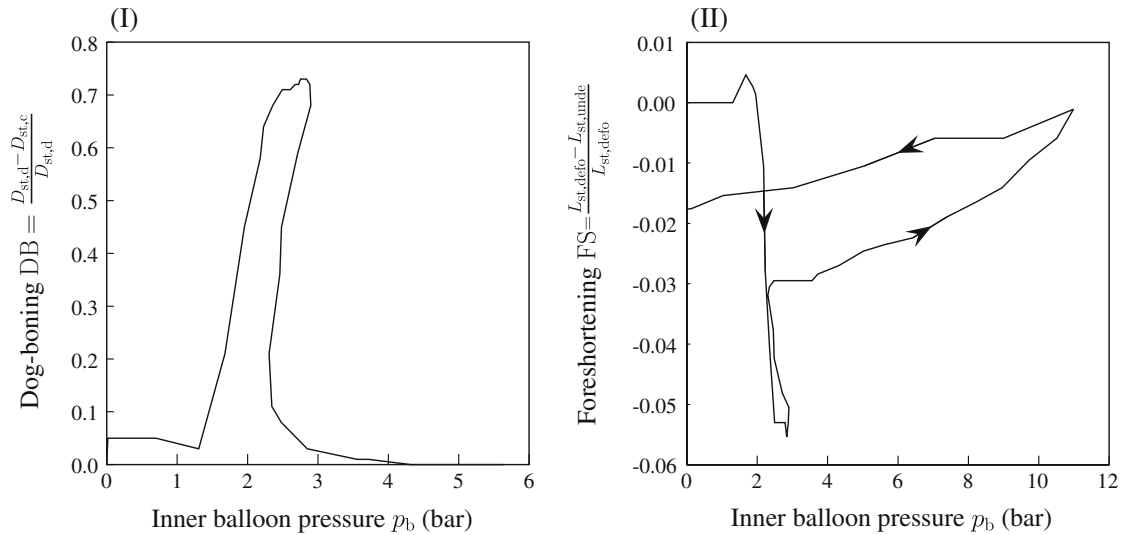


**FIGURE 6.** Phenomena that occur during the dilation of an Express LD stent: dog-boning DB (I)—the distal diameter  $D_{st,d}$  of the stent expands faster than the central diameter  $D_{st,c}$  until the burst opening of the central segments starts (at  $p_b^* = 2.90$  bar), and the stent obtains gradually a cylindrical shape; foreshortening FS (II)—during increase of the inner balloon pressure  $p_b$  the length  $L_{st,defo}$  of the stent initially shrinks. As the stent becomes cylindrical, it elongates, but does not reach its undeformed length  $L_{st,unde}$  in the fully deflated state.

Fig. 6(II). Due to the cylindrical geometry of the stent and the dog-boning, inflation of the balloon-stent system leads to a decrease in stent length. The shortening reaches its maximum value as the dog-boning reaches its maximum as well (Figs. 6(I–II)), i.e., at the burst opening pressure load of the stent’s distal segments. In addition, as the load increases to the stent’s operational pressure ( $\approx 11$  bar), the stent elongates

from its compressed configuration. Finally, the removal of the pressure load leads to an axial contraction of the stent ( $\lambda_z = 0.98$  for the Express LD stent). All stents exhibit negative foreshortening (dilated configuration shorter than the undeformed), except for the Racer stent. A positive value for the foreshortening is noted in this case, meaning that the stent is longer after its circumferential expansion.

**TABLE 2. Experimental results obtained during and after the inflation and deflation of six balloon-expandable stent systems (compare with Table 1).**

| Product             | $p_b^*$ (bar) | $DB_{max}$ (-) | $FS_{max}$ (-) | RE (%) |
|---------------------|---------------|----------------|----------------|--------|
| Express Vascular LD | 2.90          | 0.73           | -0.06          | 1.5    |
| Express Vascular SD | 4.35          | 0.67           | -0.14          | 1.1    |
| Palmaz Genesis      | 3.30          | 0.54           | -0.04          | 3.8    |
| Genesis Opti Pro    | 3.66          | 0.62           | -0.10          | 0.1    |
| Bridge Assurant     | 2.39          | 0.65           | -0.05          | 4.5    |
| Racer               | 3.32          | 0.52           | +0.02          | 5.1    |

The burst opening pressure  $p_b^*$  (in bar) for the central segments of each stent, the maximum values for the dog-boning  $DB_{max}$  and the foreshortening  $FS_{max}$ , and the elastic recoil RE (in percent) are given.

In Table 2, the burst opening pressure  $p_b^*$ , the maximum dog-boning  $DB_{max}$ , the maximum foreshortening  $FS_{max}$  and the final central radial recoil RE (in percent) are given for each of the six stents. As expected, the Express Vascular LD shows the largest dog-boning due to its larger circumferential stretch relative to the other stents. The Express Vascular SD contracts axially more than any other stent, while, as previously noted, the Racer stent showed the only positive value of foreshortening. In addition, the maximum central radial recoil was measured in the Racer stent when the balloon catheter is removed.

### Inflation of Balloon Catheters

After performing experiments on the complete balloon-stent systems, the balloons are detached from the plastically deformed, expanded stents, and used for further tests. To perform inflation tests of the detached balloons, the same experimental setup is used. Changes in the length and the diameter of the balloon catheter are recorded during a gradual increase of the inner balloon pressure.

Experimental results reveal a complex deformation mechanism for all six balloon catheters. For example, Fig. 7 shows the relationship between inner balloon pressure  $p_b$  and the balloon diameter  $D_b$  for the balloon catheter obtained from the Bridge Assurant stent system. From this figure, three deformation states of the balloon are evident. Initially, the balloon is folded into an *s*- or *z*-shaped form and has an average (reference) diameter  $D_{b,I}$  (state ①). For this specific balloon catheter  $D_{b,I}$  is assumed to be 2.0 mm. Under low pressures (up to approximately 0.5 bar), the unfolding of the balloon takes place. In this phase, the balloon expands noticeably circumferentially from its initial (complex) configuration, and obtains an almost fully cylindrical shape with diameter  $D_{b,II}$  (state ②). For the same Bridge Assurant balloon catheter,  $D_{b,II}$  is 6.22 mm at state ②. Due to the folded shape of the

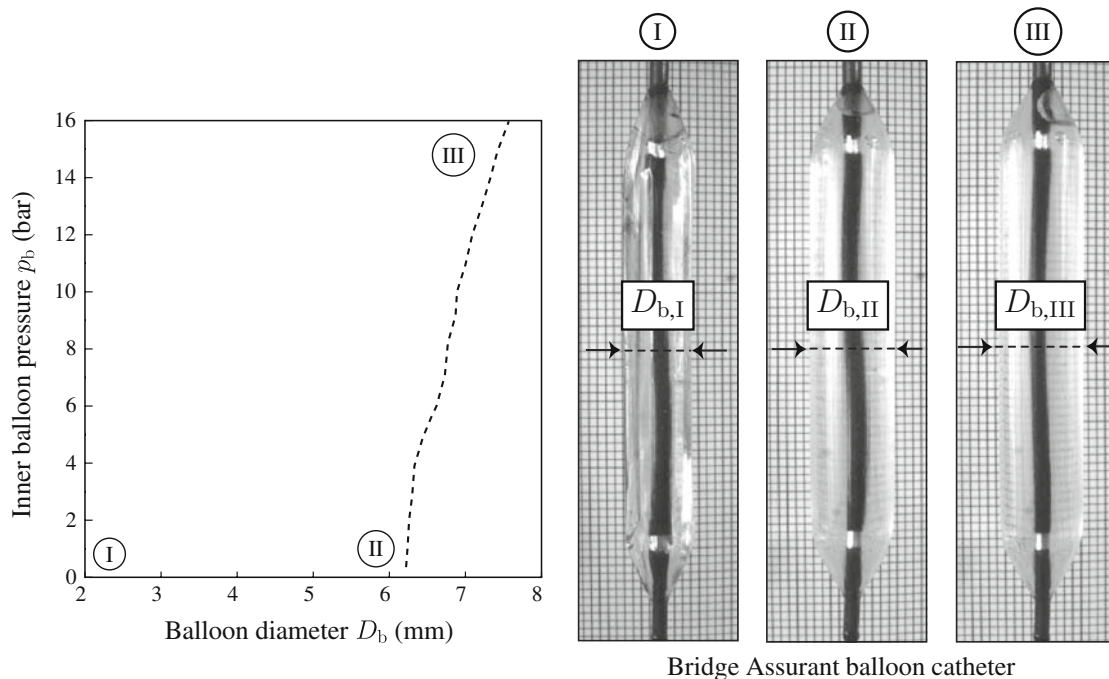


**FIGURE 7. Inner balloon pressure  $p_b$  vs. balloon diameter  $D_b$  during the inflation of a balloon catheter used for the Bridge Assurant product, and three photographs of characteristic deformation states of the balloon. Initially, at low pressure load, the folded balloon expands rapidly from its average (reference) diameter  $D_{b,I}$  (at 2.0 mm) to a diameter  $D_{b,II}$  (at approximately 0.5 bar and 6.22 mm), and obtains an almost fully cylindrical shape (phase ①). At the specific diameter  $D_{b,II}$ , the balloon catheter exposes circumferentially a (relatively linear) stiffening behavior. As the pressure load increases, the balloon slightly continues to expand, up to its final diameter  $D_{b,III}$  (phase ① → ③).**

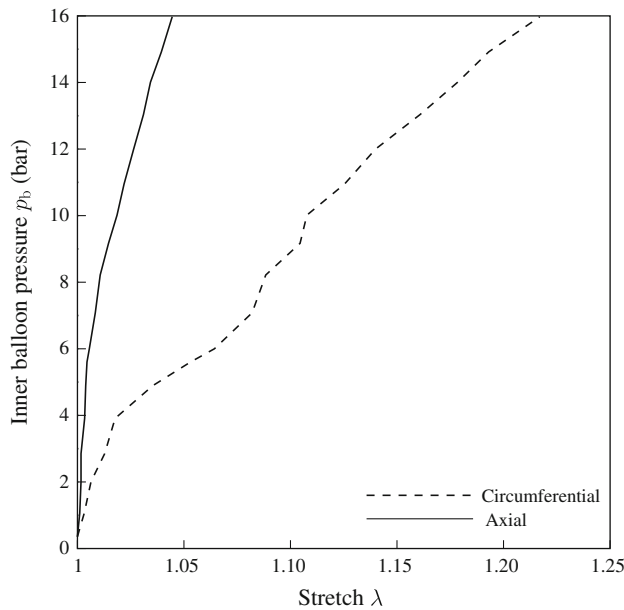


**FIGURE 8.** Inner balloon pressure  $p_b$  over axial and circumferential stretches for a balloon catheter obtained from the Bridge Assurant stent system. The two curves, shown between state ① and ③ (the reference state is state ② where the catheter has obtained an almost fully cylindrical shape), indicate a dominant anisotropic deformation mechanism, which is the same for all six investigated balloon catheters (see Table 1).

balloon, its diameter cannot be clearly defined and measured during the phase ①  $\rightarrow$  ②. Thus, the change of diameter over the pressure load during this phase is not shown in the diagram of Fig. 7. As the pressure increases to the operational value, small changes are noted in the diameter of the balloon. In other words, after a specific pressure (stretch) limit, the balloon displays a significant circumferential stiffening behavior. At the end of the inflation (state ③) the diameter of the balloon is  $D_{b,III}$  ( $=7.57$  mm). This diameter also defines the stent's expanded diameter.

A closer examination of the three balloon deformation states (①, ②, ③) shows that, despite the prominent circumferential expansion of the balloon, no significant changes take place in the axial direction (see Fig. 7). Hence, the circumferential compliance of the balloon catheter is higher than that of the axial direction during the inflation procedure. This claim is additionally supported by the curves shown in Fig. 8, where the inner balloon pressure  $D_b$  is plotted against the axial and circumferential stretches  $\lambda$  of the balloon for the phase ②  $\rightarrow$  ③, at which the balloon is already cylindrical. For the Bridge Assurant balloon catheter, it is evident that the stretches in the circumferential direction are higher than in the axial direction, even after the balloon has reached the diameter  $D_{b,II}$ . The circumferential stretch at state ③ is about 20% higher than that in the axial direction (note that due to the

folding mechanism the stretch refers to the whole structure and may not necessarily reflect the stretch in the actual balloon material).

The deformation mechanisms described above are the same for all six balloon catheters, and very similar graphs to the ones in Figs. 7 and 8 are obtained. Nevertheless, each balloon exhibits different diameters  $D_{b,II}$  and  $D_{b,III}$ . For example, for the Bridge Assurant system  $D_{b,II} = 6.22$  mm, while for the Express Vascular LD system  $D_{b,II} = 8.85$  mm, and for the Palmaz Genesis system  $D_{b,II} = 6.35$  mm.

## NUMERICAL MODELING

We present a finite element model for the inflation procedure of balloon catheter-stent systems in more detail and apply the model to analyze the Bridge Assurant system. We outline a parametric algorithm to generate the stent geometry and review a recently proposed cylindrically orthotropic model for the balloon, and an efficient contact algorithm for elastic bodies undergoing large deformations and sliding. The constitutive model for the balloon and the contact algorithm were implemented into the multipurpose Finite Element Analysis Program FEAP.<sup>52</sup> The inputs are material parameters for the balloon material model, and are derived from the inflation experiments described previously. The numerical results are presented in terms of pressure–diameter diagrams, and compared with experimental data.

### Stent Geometry and Material

The six stent geometric models are generated by means of a developed parametrization algorithm. Parametric design is a powerful technique in engineering when numerical optimization is used to generate the ‘optimal’ design of a product. In our case, the algorithm enables an efficient variation of the stents’ configurations and the generation of new stent designs just by varying their geometric structure.

The required input data consist of a set of geometric parameters, which are indicated in Fig. 9 along with the generated models of the undeformed configurations of three stents.

The required geometric parameters are:

- (i) number  $n_u$  of the units for each segment (could vary among segments of the same stent, as it is the case for the Express stents),
- (ii) lengths  $l_{u,a}$  and  $l_{u,b}$  of the units,
- (iii) wave lengths  $w_{u,a}$  and  $w_{u,b}$  of the units,
- (iv) distance  $l_{s,c}$  between two consequent segments, and
- (v) diameter  $D_{st}$  and the length  $L_{st}$  of the stent.

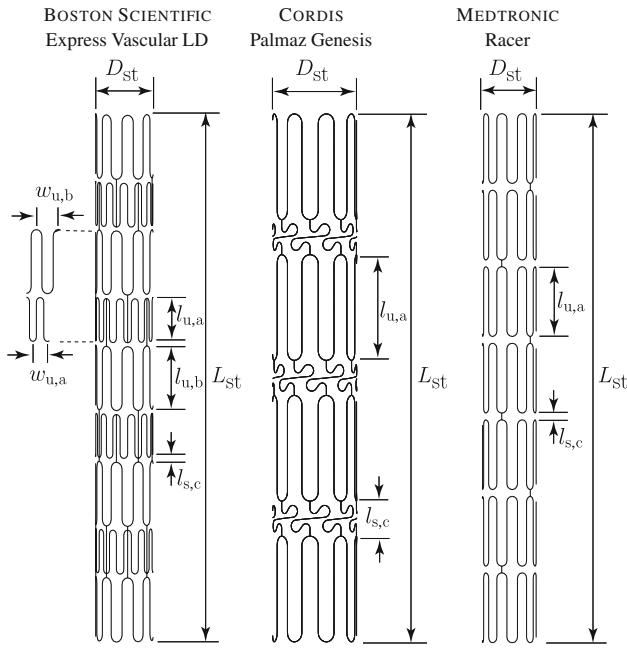


**FIGURE 9.** Geometric models of the undeformed configurations of three stent products (compare with Table 1). The stent geometries are generated by means of a developed parametrization algorithm enabling an efficient variation of the stents' configurations and the generation of new stent designs. The required set of geometric parameters are: the number  $n_u$ , the lengths  $l_{u,a}$  and  $l_{u,b}$ , and the wave lengths  $w_{u,a}$  and  $w_{u,b}$  of the units for each segment, the distance  $l_{s,c}$  between two consecutive segments, and the diameter  $D_{st}$  and the length  $L_{st}$  of the stent.

The output of the parametrization algorithm is the geometric model of the stent and the related finite element mesh. The generated mesh consists of two-node, large displacement, and large rotation 3D frame elements.<sup>25</sup> The density of the finite element mesh may be defined by additional user-specified parameters that control the number of nodes in the axial and circular parts of the units, and the number of nodes at the links.

This numerical study focuses particularly on the Bridge Assurant stent system, which is made out of stainless steel 316L. Hence, we adopt a neo-Hookean model for the elastic domain, and the von Mises-Hill plasticity model ( $J_2$  flow theory) with linear hardening for the inelastic domain of the stent material. We choose a Young's modulus  $E = 193.0$  GPa, a Poisson's ratio  $\nu = 0.3$ , a yield stress  $\sigma_y = 300.0$  MPa, and a linear hardening modulus  $H_{iso} = 2.0$  GPa.<sup>2</sup>

### Balloon Geometry and Material

The deformation patterns of angioplasty balloons under inner pressure are particularly complex, as is demonstrated by the experimentally observed anisotropic behavior (see Figs. 7 and 8). The balloon's initial folded configuration and the unfolding phase add another degree of complexity to the modeling process. To

incorporate these phenomena at least phenomenologically, a cylindrically orthotropic model, as presented in the recent papers by Kiousis *et al.*<sup>27,28</sup> is adopted. The model is based on the theory of the mechanics of fiber-reinforced composites, as introduced by Holzapfel *et al.*,<sup>23</sup> and is briefly summarized in the subsequent part of this section.

The folded initial shape of the balloon is not taken into account and the balloon is modeled as a perfect cylinder. The balloon material is assumed to be incompressible and much stiffer axially than circumferentially. According to the experimental data, the mechanical response of the balloon in the circumferential direction is considered to be very soft up to a stretch limit. Beyond this limit, the stiffness of the balloon in the circumferential direction increases significantly. To capture this peculiar balloon response, two orthogonal material axes are introduced. They are characterized by the unit vectors  $\mathbf{a}_{01}$  and  $\mathbf{a}_{02}$ , which are oriented in the axial and circumferential directions of the undeformed balloon configuration, respectively.

For the balloon material we assume the existence of a strain-energy function defined per unit reference volume, and allow an additive decomposition of that function into volumetric and isochoric parts.<sup>22</sup> While the volumetric contribution is motivated mathematically (described by a penalty function), the isochoric contribution, labeled as  $\bar{\Psi}$ , is now described in more detail. We assume a separation of  $\bar{\Psi}$  into an isotropic part  $\bar{\Psi}_{iso}$ , associated with the deformation of the matrix material, and an anisotropic part  $\bar{\Psi}_{aniso}$ , which takes care of the anisotropic behavior of the balloon response. The two-term potential may be written as

$$\bar{\Psi}(\bar{\mathbf{C}}, \mathbf{a}_{01}, \mathbf{a}_{02}) = \bar{\Psi}_{iso}(\bar{\mathbf{C}}) + \bar{\Psi}_{aniso}(\bar{\mathbf{C}}, \mathbf{a}_{01}, \mathbf{a}_{02}), \quad (4)$$

where  $\bar{\mathbf{C}} = J^{-2/3} \mathbf{F}^T \mathbf{F}$  is the modified right Cauchy-Green tensor,  $J > 0$  is the local volume ratio, and  $\mathbf{F}$  is the deformation gradient.<sup>22</sup> By introducing the structure tensors  $\mathbf{A}_1 = \mathbf{a}_{01} \otimes \mathbf{a}_{01}$  and  $\mathbf{A}_2 = \mathbf{a}_{02} \otimes \mathbf{a}_{02}$ , Eq. (4) may be written in the reduced form<sup>23</sup>

$$\bar{\Psi}(\bar{\mathbf{C}}, \mathbf{A}_1, \mathbf{A}_2) = \bar{\Psi}_{iso}(\bar{I}_1) + \bar{\Psi}_{aniso}(\bar{I}_4, \bar{I}_6), \quad (5)$$

with the first invariant  $\bar{I}_1 = \text{tr} \bar{\mathbf{C}}$  of  $\bar{\mathbf{C}}$ , and the two invariants  $\bar{I}_4 = \bar{\mathbf{C}} : \mathbf{A}_1$  and  $\bar{I}_6 = \bar{\mathbf{C}} : \mathbf{A}_2$  of  $\bar{\mathbf{C}}, \mathbf{A}_1$  and  $\bar{\mathbf{C}}, \mathbf{A}_2$ , respectively. The invariants  $\bar{I}_4$  and  $\bar{I}_6$  are the squares of the stretches in the directions of  $\mathbf{a}_{01}$  and  $\mathbf{a}_{02}$ , respectively, and therefore have a clear physical interpretation. From the above equation it is obvious that anisotropy arises only due to  $\bar{I}_4$  and  $\bar{I}_6$ .

The isotropic response of the matrix material is determined through a neo-Hookean model of the form  $\bar{\Psi}_{iso} = \mu(\bar{I}_1 - 3)$ , where  $\mu > 0$  is a stress-like material parameter. The anisotropic contribution  $\bar{\Psi}_{aniso}$  to the strain-energy function is described as<sup>27</sup>

$$\bar{\Psi}_{\text{aniso}}(\bar{I}_4, \bar{I}_6) = \sum_{i=4,6} \frac{d_{1,i}}{n} (\bar{I}_i - d_{2,i})^n. \quad (6)$$

The parameters  $n$  and  $d_{2,i}$ ,  $i = 4,6$ , are dimensionless, while  $d_{1,i}$ ,  $i = 4,6$ , have dimensions of stress. With this function, the stiffness in each direction is described by  $d_{1,i}$ , while  $d_{2,i}$  defines the initiation of the balloon's stiffening behavior (axially and circumferentially).

To illustrate the accuracy of the described material model, a numerical analysis of the Bridge Assurant balloon catheter is performed and compared with the experimental data. The diameter and length of the balloon in the undeformed configuration are assumed to be 2.0 and 20.0 mm, respectively. The balloon is discretized by eight-node hexahedral elements. To account for incompressibility a mixed finite element formulation is used. The upper and lower faces of the balloon are fixed in all directions. The expansion of the balloon catheter is performed by a pressure load, which acts at the deformed inner boundary surface of the balloon, and which is deformation dependent. To match the characteristic mechanical response, the parameter  $d_{2,4}$  is chosen equal to 1. In the case of the Bridge Assurant balloon, the diameter  $D_{b,\text{II}}$  at state ② is 6.22 mm, which corresponds to a circumferential stretch of 3.11. The value  $d_{2,6}$ , describing the initiation of the stiffening in the circumferential direction, is chosen equal to 10, and the exponent in Eq. (6) is 3. The stiffness in the two material axes of the balloon is defined by the values  $d_{1,4} = 1000$  N/mm and  $d_{1,6} = 100$  N/mm, respectively, while for the isotropic part  $\mu = 100$  MPa. Figure 10 illustrates the results of the finite element simulation of the dilation process of the Bridge Assurant balloon. The solid curve represents the change of the inner balloon pressure  $p_b$  with the central diameter of the balloon. As depicted in Fig. 10, between load  $p_b = 0$  bar and  $p_b = 0.5$  bar, the balloon diameter increases considerably. This phase (①  $\rightarrow$  ②) simulates the complex unfolding of the balloon. After this phase, at state ②, the balloon stiffens circumferentially. In Fig. 10, the experimental results are illustrated by a dashed curve. As can be seen, the numerical model captures qualitatively and quantitatively the experimentally observed deformation mechanism of the balloon catheter.

#### Contact Between the Stent and the Balloon

The numerical simulation of the interaction of the stent with the balloon is a challenging nonlinear problem in computational mechanics. The main difficulties arise from the nonlinear behavior of the involved bodies, the anisotropy of the balloon catheter, the involved finite deformations and the complex three-dimensional contact interaction of the two

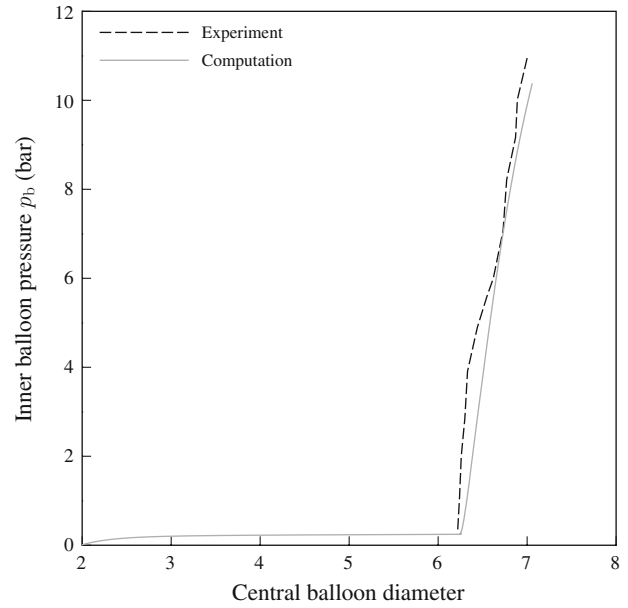


**FIGURE 10.** Experimental results in comparison with results obtained from a finite element simulation of the dilation process of the Bridge Assurant balloon analyzed with the material model (6). Inner balloon pressure  $p_b$  vs. central balloon diameter. Up to about  $p_b = 0.5$  bar the balloon diameter increases considerably and beyond that pressure the balloon stiffens circumferentially. The computational model shows good agreement with the experiments.

medical devices. There is strong evidence<sup>15,49</sup> that facet-based contact algorithms often lead to numerical problems during simulations where large deformations and bodies with arbitrary geometries are involved. Problems encountered include: oscillation of contact forces, nonrealistic pressure jumps, contact cycling, and loss of quadratic convergence of the nonlinear solution scheme.

To overcome these numerical instabilities, the contact algorithm developed and documented in Kioussis *et al.*<sup>27</sup> is adopted here. In this context, the stent is considered as the contractor and the balloon as the target body. By applying the node-to-surface approach, the stent is described through its (finite element) nodes and the balloon by  $C^2$ -continuous surfaces. While several parametrization methods have been implemented into contact algorithms,<sup>42,48,49</sup> the discussed technique makes use of uniform cubic B-splines surfaces<sup>43</sup> mathematically described as

$$\mathbf{S}(u, v) = \sum_{i=1}^4 \sum_{j=1}^4 B_i(u) B_j(v) \mathbf{P}_{i,j}, \quad 0 \leq u, v \leq 1, \quad (7)$$

where  $u$  and  $v$  are convective coordinates,  $\mathbf{P}_{i,j}$ ,  $i, j = 1, \dots, 4$  is a structured, bidirectional mesh of  $4 \times 4$  control points, and  $B_k$ ,  $k = 1, \dots, 4$  are cubic basis functions of the form

$$\begin{aligned}
 B_1(t) &= (1 - 3t + 3t^2 - t^3)/6, \\
 B_2(t) &= (4 - 6t^2 + 3t^3)/6, \\
 B_3(t) &= (1 + 3t + 3t^2 - 3t^3)/6, \\
 B_4(t) &= t^3/6,
 \end{aligned}
 \tag{8}$$

where  $t$  stands for  $u$  or  $v$ . In the present approach, the control points  $\mathbf{P}_{i,j}$  are formed by the superficial element nodes of the target body, i.e., the balloon. The uniform cubic B-splines have useful properties such as  $C^2$ -continuity and local support, and the normal vector changes smoothly over the boundaries of surfaces. Therefore, the application of uniform cubic B-splines leads to a robust contact algorithm. For more details on the implementation of the parametrization scheme into a numerical framework (especially into FEAP<sup>52</sup>), the reader is referred to the original work by Kiousis *et al.*<sup>27</sup>

### Finite Element Model of the Balloon Catheter-Stent System

Figure 11(I) shows the finite element model of the Bridge Assurant balloon catheter-stent system. The total number of degrees of freedom is approximately 6000. The upper and lower faces of the balloon are fixed in all directions. To each node of the stent, an axial stiffness is added. This restricts axial rigid motion at the nodes and, in addition, incorporates (a phenomenological) friction between the inner side of the stent and the outer surface of the balloon. Friction was not explicitly implemented because a reliable friction coefficient is not yet known. The pressure boundary loading is applied at the inner surface of the balloon. The gradual increase of the inner pressure inflates the balloon, which comes into contact with the stent, and consequently, leads to full expansion of the system. The contact constraint is enforced by the penalty method.

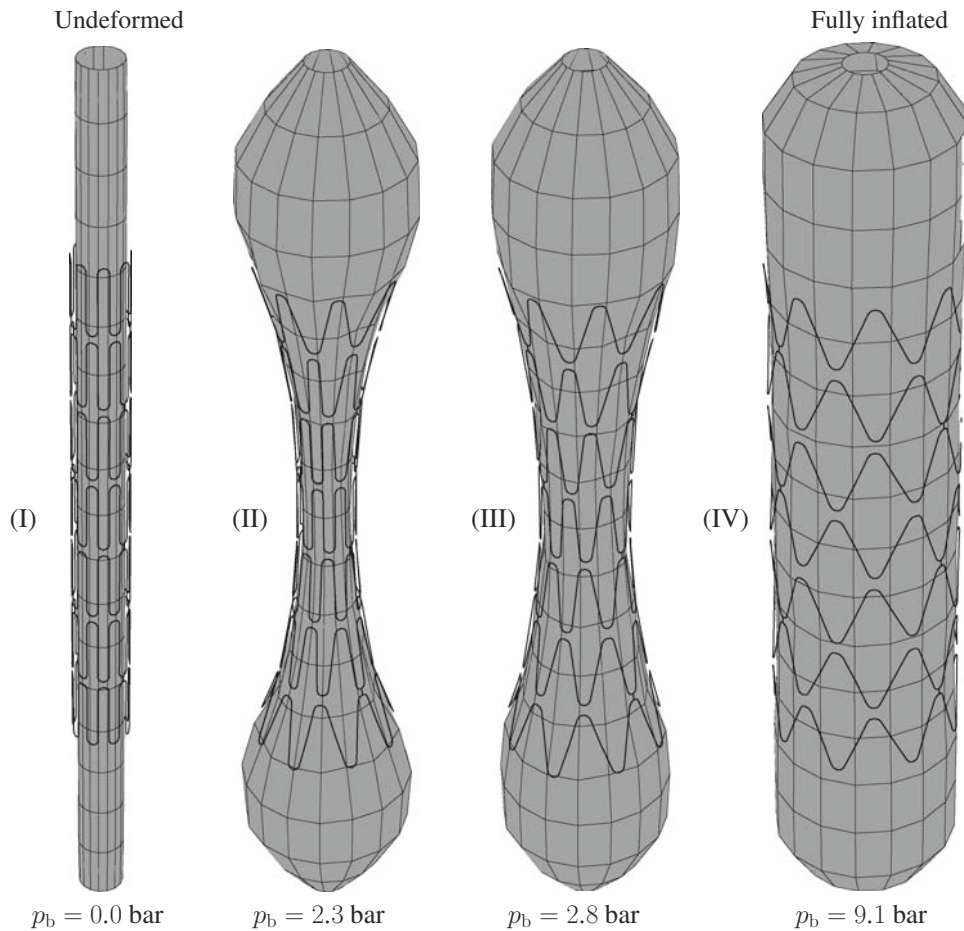


**FIGURE 11.** Finite element model of the Bridge Assurant balloon catheter-stent system (I). Deformed configurations of the system at different pressure levels (II), (III), (IV) (the upper and lower faces of the balloon are fixed in all directions, and pressure boundary loading is applied at the inner surface of the balloon). The numerical model successfully reproduces the experimentally observed deformation mechanisms, for example, the dog-boning (compare with Fig. 3).

### Numerical Results of the Inflation Process

Figure 11(II–IV) shows results of the finite element simulation in terms of the deformed configurations of the Bridge Assurant balloon catheter-stent system at three load levels during inflation process. The computation points out that the distal cells of the stent are more compliant than the central cells, which is in agreement with experimental observation (the edges of the stent expand faster than the central region, i.e., dog-boning, see Fig. 11(II–III)). More specifically, for  $p_b = 2.3$  bar (Fig. 11(II)) the cell in the central region of the stent is almost unexpanded, since the pressure load has not yet reached the burst opening value, which is at  $p_b^* = 2.39$  for the Bridge Assurant system (see Table 2). Meanwhile, the distal segments have acquired a significantly larger diameter. As the pressure load increases (Fig. 11(III)), the central segment expands, and at  $p_b = 9.1$  bar (Fig. 11(IV)) the stent obtains its fully expanded cylindrical shape.

To validate the accuracy and efficacy of the employed finite element model and the contact algorithm, we compare the pressure–diameter diagrams obtained from the experiments and the numerical simulation (see Fig. 12(I, II)). Overall, the numerical results (solid curves) are in satisfactory agreement with the experimental data (dashed curve, from Fig. 5). The computation is able to precisely capture the initial expansion phase ㉑ → ㉒ of the balloon-expandable stent system for both the central and the distal diameter of the system. In addition, the numerical results for the distal diameter of the system during the dilation phase ㉒ → ㉓

agree also quite well with the experimental data. This is not the case for the central diameter because Newton iterations are used to solve the algebraic equations. One possible modification to improve the accuracy of the simulation (according to the experimental results of the central system diameter during dilation phase) is the application of an arc-length method. Thereby, a length of a specified load–displacement path may be provided instead of a pressure load step.

At the final phase ㉓ → ㉔ of the system’s inflation, where the balloon stiffens circumferentially, the numerical model demonstrates a slightly stiffer behavior when compared to the experimental data for the region  $p_b \in [5, 10]$  bar (about 7% difference). A closer review of Fig. 5 (experimental results) reveals that several balloon-stent systems demonstrate two stiffening regions within the phase ㉓ → ㉔, which is clearly visible for the Bridge Assurant system in Fig. 12. It is apparent that at a pressure load of about  $p_b = 5.0$  bar, a transition of the balloon-stent’s circumferential stiffness takes place and the overall system becomes more compliant. The numerical model, while able to track the initial experimental results, is not able to mimic this transitional zone of the (circumferential) stiffness.

### SUMMARY AND CONCLUSION

The present paper analyzed the mechanical response of six vascular balloon catheter-stent systems, and of angioplasty balloons detached from the catheter-stent

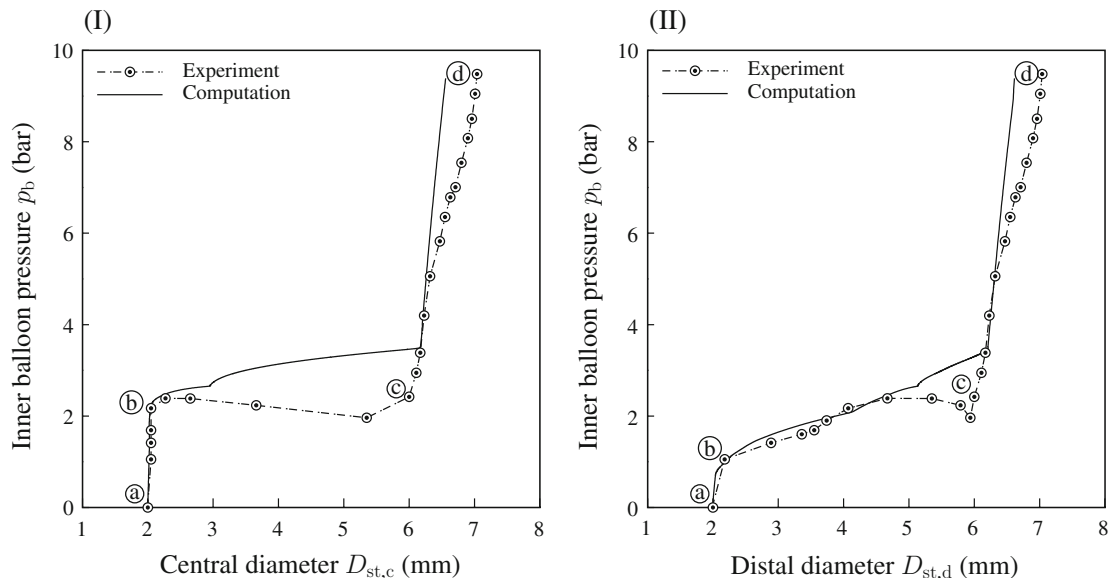


FIG. 12. Comparison of the experimental and the numerical results for the dilation of the Bridge Assurant balloon-stent system; change of the inner balloon pressure  $p_b$  vs. the central diameter  $D_{st,c}$  (I), and the distal diameter  $D_{st,d}$  (II). Overall, the numerical results (solid curves) are in satisfactory agreement with the experimental data (dashed curve, from Fig. 5).

systems, during inflation. The analysis was initially approached from an experimental point of view. Next, guided by the experimental data, a finite element framework was developed which is able to reproduce the typical mechanical characteristics of catheter-stent systems.

Cooperations were established with three stent manufacturers, and six current stent products were acquired (product details are summarized in Table 1). After recording the stent structures and dimensions, the balloon-stent systems underwent inflation tests. A pneumatic-hydraulic experimental setup was built (Fig. 2) to apply pressure inside the balloon catheters, while simultaneously recording the loads and deformed states of the balloon-expandable stents during inflation. Postprocessing of the experimentally obtained data and images (shown for example for an Express Vascular LD balloon-stent system in Fig. 3), made it possible to extract the characteristic pressure-diameter diagrams for each stent (Figs. 4 and 5). These images and diagrams reveal that during inflation of the balloon-stent systems, the overall deformation path can be subdivided into three characteristic phases, and that phenomena such as dog-boning and foreshortening take place (Fig. 6). Table 2 summarizes additional important information including the burst opening pressure, the maximum dog-boning and foreshortening values, and the elastic recoil.

To acquire a more thorough understanding of the mechanical behavior of modern balloon catheters (detached from the stents), the same experimental setup and protocol were used. Findings underline an almost bi-linear and anisotropic deformation mechanism, which is the same for all investigated balloon catheters (Figs. 7 and 8). The balloons showed significant axial stiffness during the inflation, while in the circumferential direction they were very compliant (unfolding phase) for pressure levels between 0 and approximately 0.5 bar. However, at higher pressure loads pronounced stiffening occurred.

Subsequently, a finite element model for simulating inflation of the balloon and its interaction with the stent was presented, focusing on the Bridge Assurant stent system. A parametrization algorithm was developed to generate geometric models of the undeformed stent configurations (see Fig. 9). Deformation of the stent was taken into consideration by an elastoplastic material model. To describe the unfolding process of the balloon, and the circumferential stiffening behavior in a phenomenological way, a nonlinear anisotropic model was adopted.<sup>27,28</sup> The computational model for the balloon was shown to be in good agreement with the experimental results (Fig. 10). The contact interaction of the two bodies was modeled by means of a contact algorithm based on a uniform cubic B-spline

surface parametrization. The penalty method was applied to impose the contact constraint. The finite element model reproduced the experimental data in a robust way (Fig. 11). Comparative study showed good agreement between the pressure-diameter diagrams generated from the experimental data and the simulation (Fig. 12). The model successfully captured the mechanics of the balloon-stent system under dilation. However, it should be noted that the pressure drop during the burst opening phase could not be captured by the applied numerical methodology.

The proposed experimental and computational approach demonstrated suitability for better analyzing commercially available vascular balloon catheter-stent systems, and also developing new stent designs. The presented methodology identified stents with maximum values of dog-boning and foreshortening. Even though a direct comparison of these specific products was not feasible (since the stents are of different sizes and target lesions of different diameters and lengths), the computational model can serve as a test bed for new stent geometries. New designs can *a priori* be tested in this numerical platform, and can be evaluated in terms of final expansion diameter, dog-boning or foreshortening. In such a way, the presented model can be a valuable tool for stent manufacturers. In addition, studies of the morphologic changes in lesions during *in vitro* angioplasty using certain imaging modalities and image processing<sup>3</sup> and/or experimentally validated models for the interaction with a lesion<sup>24,28,31,32</sup> can assist the development of accurate and reliable patient-specific simulations. In this way, more information on arterial damage can be provided in the future.

However, there are still limitations that should be addressed in the near future. The presented study did not consider the interaction of the medical devices with the vascular wall. The balloon-stent systems were not tested in the application environment, i.e., inside an atherosclerotic arterial wall. The design of such an experiment could provide information on the damage induced by the stent struts on the endothelial layer. Such an attempt however exceeds the aims of the current work. Crimping of the stent to the balloon catheter was not simulated, and hence the residual stresses and strains resulting from this procedure were not considered. It is noted, however, that the results of the recent computational study by De Beule *et al.*<sup>9</sup> show that the crimping procedure has a minor influence on the overall expansion of the stent. The undeformed configuration of the balloon catheter is considered to be uniform and cylindrical, and its folded shape is not modeled. However, the adopted nonlinear model manages to successfully simulate the unfolding phase of the balloon in a phenomenological way. In addition, the presented computational model

did not incorporate microstructural effects of the stent. The average grain size of stainless steel is almost of the same order of magnitude as the stent's strut thickness (approximately 150  $\mu\text{m}$ ). Therefore, a continuum mechanical model may be questionable. Note that the paper by McGarry *et al.*<sup>33</sup> analyzes microscale mechanical phenomena of the stent material behavior using physically based crystal plasticity theory rather than phenomenological plasticity theory.

The authors hope, despite of the mentioned limitations, that this analysis assists the biomechanics and medical community in future numerical investigations toward optimization of the stenting technique.

### ACKNOWLEDGMENTS

The authors are indebted to the Swedish subsidiaries of Boston Scientific, Cordis, and Medtronic for generously providing the vascular stent products investigated in this work.

### REFERENCES

- <sup>1</sup>Allender, St., P. Scarborough, V. Peto, M. Rayner, J. Leal, R. Luengo-Fernandez, and A. Gray. European Cardiovascular Disease Statistics, 2008 Edition. British Heart Foundation Health Promotion Research Group and Health Economic Research Centre, Department of Public Health, University of Oxford, 2008. [www.heartstats.org](http://www.heartstats.org).
- <sup>2</sup>American Society for Metals International Handbook Committee. Metals Handbook. OH: ASM International, 1999.
- <sup>3</sup>Auer, M., R. Stollberger, P. Regitnig, F. Ebner, and G. A. Holzapfel. A methodology to study the morphologic changes in lesions during *in vitro* angioplasty using MRI and image processing. *Med. Image Anal.* 12:163–173, 2008.
- <sup>4</sup>Barragan, P., R. Rieu, V. Garitey, P. O. Roquebert, J. Sainous, M. Silvestri, and G. Bayet. Elastic recoil of coronary stents: a comparative analysis. *Catheter Cardiovasc. Interv.* 50:112–119, 2000.
- <sup>5</sup>Brauer, H., J. Stolpmann, H. Hallmann, R. Erbel, and A. Fischer. Measurement and numerical simulation of the dilatation behaviour of coronary stents. *Mat.-wiss. u. Werkstofftechn.* 30:876–885, 1999.
- <sup>6</sup>Carrozza, J. P., R. E. Kuntz, M. J. Levine, R. M. Pomerantz, R. F. Fishman, M. Mansour, C. M. Gibson, C. C. Senerchia, D. J. Diver, R. D. Safian, *et al.* Angiographic and clinical outcome of intracoronary stenting: immediate and long-term results from a large single-center experience. *J. Am. Coll. Cardiol.* 20:328–337, 1992.
- <sup>7</sup>David Chua, S. N., B. J. Mac Donald, and M. S. J. Hashmi. Finite element simulation of stent and balloon interaction. *J. Mat. Proc. Techn.* 143–144:591–597, 2003.
- <sup>8</sup>Degertekin, M., E. Regar, K. Tanabe, P. C. Smits, W. J. van der Giessen, S. G. Carlier, P. de Feyter, J. Vos, D. P. Foley, J. M. Ligthart, J. J. Popma, and P. W. Serruys. Sirolimus-eluting stent for treatment of complex in-stent restenosis: the first clinical experience. *J. Am. Coll. Cardiol.* 41:184–189, 2003.
- <sup>9</sup>De Beule, M., P. Mortier, R. Van Impe, B. Verheghe, P. Segers, and P. Verdonck. Plasticity in the mechanical behaviour of cardiovascular stents during stent preparation (crimping) and placement (expansion). *Key Eng. Mater.* 340–341:847–852, 2007.
- <sup>10</sup>De Beule, M., R. Van Impe, B. Verheghe, P. Segers, and P. Verdonck. Finite element analysis and stent design: reduction of dogboning. *Technol. Health Care* 14:233–241, 2006.
- <sup>11</sup>Donnelly, E. W., M. S. Bruzzi, T. Connolley, and P. E. McHugh. Finite element comparison of performance related characteristics of balloon expandable stents. *Comput. Meth. Biomech. Biomed. Eng.* 10:103–110, 2007.
- <sup>12</sup>Duda, S. H., J. Wiskirchen, G. Tepe, M. Bitzer, T. W. Kaulich, D. Stoeckel, and C. D. Claussen. Physical properties of endovascular stents: an experimental comparison. *J. Vasc. Interv. Radiol.* 11:645–654, 2000.
- <sup>13</sup>Dumoulin, C., and B. Cochelin. Mechanical behaviour modelling of balloon-expandable stents. *J. Biomech.* 33:1461–1470, 2000.
- <sup>14</sup>Edelman, E. R., and C. R. Rogers. Pathobiologic responses to stenting. *Am. J. Cardiol.* 81:4E–6E, 1998.
- <sup>15</sup>El-Abbasi, N., S. A. Meguid, and A. Czekanski. On the modelling of smooth contact surfaces using cubic splines. *Int. J. Numer. Meth. Eng.* 50:953–967, 2001.
- <sup>16</sup>Etave, F., G. Finet, M. Boivin, J. C. Boyer, G. Rioufol, and G. Thollet. Mechanical properties of coronary stents determined by using finite element analysis. *J. Biomech.* 34:1065–75, 2001.
- <sup>17</sup>Farb, A., G. Sangiorgi, A. J. Carter, V. M. Walley, W. D. Edwards, R. S. Schwartz, and R. Virmani. Pathology of acute and chronic coronary stenting in humans. *Circulation* 99:44–52, 1999.
- <sup>18</sup>Fattori, R., and T. Piva. Drug-eluting stents in vascular intervention. *Lancet* 361:247–249, 2003.
- <sup>19</sup>Hoffmann, R., G. S. Mintz, G. R. Dussaillant, J. J. Popma, A. D. Pichard, L. F. Satler, K. M. Kent, J. Griffin, and M. B. Leon. Patterns and mechanisms of in-stent restenosis. A serial intravascular ultrasound study. *Circulation* 94:1247–1254, 1996.
- <sup>20</sup>Hoffmann, R., G. S. Mintz, R. Mehran, K. M. Kent, A. D. Pichard, L. F. Satler, and M. B. Leon. Tissue proliferation within and surrounding Palmaz-Schatz stents is dependent on the aggressiveness of stent implantation technique. *Am. J. Cardiol.* 83:1170–1174, 1999.
- <sup>21</sup>Hoher, M., J. Wöhrle, C. Grebe, M. Kochs, H. H. Osterhues, V. Hombach, and A. B. Buchwald. A randomized trial of elective stenting after balloon recanalization of chronic total occlusions. *J. Am. Coll. Cardiol.* 34:722–729, 1999.
- <sup>22</sup>Holzapfel, G. A. *Nonlinear Solid Mechanics. A Continuum Approach for Engineering*. Chichester: John Wiley & Sons, 2000.
- <sup>23</sup>Holzapfel, G. A., T. C. Gasser, and R. W. Ogden. A new constitutive framework for arterial wall mechanics and a comparative study of material models. *J. Elasticity* 61:1–48, 2000.
- <sup>24</sup>Holzapfel, G. A., M. Stadler, and T. C. Gasser. Changes in the mechanical environment of stenotic arteries during interaction with stents: computational assessment of parametric stent design. *J. Biomech. Eng.* 127:166–180, 2005.
- <sup>25</sup>Ibrahimbegović, A., and M. Al Mikdad. Finite rotations in dynamics of beams and implicit time-stepping schemes. *Int. J. Numer. Meth. Eng.* 66:781–814, 1998.

- <sup>26</sup>Iijima, R., J. Mehilli, A. Schömig, and A. Kastrati. Clinical evidence on polymer-based sirolimus and paclitaxel eluting stents. *Minerva Cardioangiol.* 54:539–555, 2006.
- <sup>27</sup>Kiousis, D. E., T. C. Gasser, and G. A. Holzapfel. Smooth contact strategies with emphasis on the modeling of balloon angioplasty with stenting. *Int. J. Numer. Meth. Eng.* 75:826–855, 2008.
- <sup>28</sup>Kiousis, D. E., T. C. Gasser, and G. A. Holzapfel. A numerical model to study the interaction of vascular stents with human atherosclerotic lesions. *Ann. Biomed. Eng.* 35:1857–1869, 2007.
- <sup>29</sup>König, A., T. M. Schiele, J. Rieber, K. Theisen, H. Mudra, and V. Klauss. Influence of stent design and deployment technique on neointima formation and vascular remodeling. *Z. Kardiol.* 91:98–102, 2002.
- <sup>30</sup>Kornowski, R., M. K. Hong, F. O. Tio, O. Bramwell, H. Wu, and M. B. Leon. In-stent restenosis: contributions of inflammatory responses and arterial injury to neointimal hyperplasia. *J. Am. Coll. Cardiol.* 31:224–230, 1998.
- <sup>31</sup>Lally, C., F. Dolan, and P. J. Prendergast. Cardiovascular stent design and vessel stresses: a finite element analysis. *J. Biomech.* 38:1574–1581, 2005.
- <sup>32</sup>Liang, D. K., D. Z. Yang, M. Qi, and W. Q. Wang. Finite element analysis of the implementation of a balloon expandable stent in a stenosed artery. *Int. J. Cardiol.* 104:314–318, 2005.
- <sup>33</sup>McGarry, J. P., B. P. O'Donnell, P. E. McHugh, and J. G. McGarry. Analysis of the mechanical performance of a cardiovascular stent design based on micromechanical modelling. *Comp. Mater. Sci.* 31:421–438, 2004.
- <sup>34</sup>McLean, D. R., and N. L. Eiger. Stent design: implications for restenosis. *Rev. Cardiovas. Med.* 3:16–22, 2002.
- <sup>35</sup>Migliavacca, F., L. Petrini, M. Colombo, F. Auricchio, and R. Pietrabissa. Mechanical behavior of coronary stents investigated through the finite element method. *J. Biomech.* 35:803–811, 2002.
- <sup>36</sup>Migliavacca, F., L. Petrini, V. Montanari, I. Quagliana, F. Auricchio, and G. Dubini. A predictive study of the mechanical behaviour of coronary stents by computer modelling. *Med. Eng. Phys.* 27:13–18, 2005.
- <sup>37</sup>Morton, A. C., D. Crossman, and J. Gunn. The influence of physical stent parameters upon restenosis. *Pathol. Biol. (Paris)* 52:196–205, 2004.
- <sup>38</sup>Moses, J. W., M. B. Leon, J. J. Popma, P. J. Fitzgerald, D. R. Holmes, C. O'Shaughnessy, R. P. Caputo, D. J. Kereiakes, D. O. Williams, P. S. Teirstein, J. L. Jaeger, R. E. Kuntz, and SIRIUS Investigators. Sirolimus-eluting stents versus standard stents in patients with stenosis in a native coronary artery. *N. Engl. J. Med.* 349:1315–1323, 2003.
- <sup>39</sup>Nikkari, S. T., and A. W. Clowes. Restenosis after vascular reconstruction. *Ann. Med.* 26:95–100, 1994.
- <sup>40</sup>Olbrich, T., and A. Murray. Assessment of computer-controlled inflation/deflation for determining the properties of PTCA balloon catheters with pressure–volume curves. *Physiol. Meas.* 22:299–308, 2001.
- <sup>41</sup>Ormiston, J. A., S. R. Dixon, M. W. Webster, P. N. Ruygrok, J. T. Stewart, I. Minchington, and T. West. Stent longitudinal flexibility: a comparison of 13 stent designs before and after balloon expansion. *Catheter Cardiovasc. Interv.* 50:120–124, 2000.
- <sup>42</sup>Padmanabhan, V., and T. A. Laursen. A framework for development of surface smoothing procedures in large deformation frictional contact analysis. *Finite Elem. Anal. Des.* 37:173–198, 2001.
- <sup>43</sup>Piegel, L. A., and W. Tiller. The NURBS Book. 2nd ed. New York: Springer-Verlag, 1997.
- <sup>44</sup>Rieu, R., P. Barragan, C. Masson, J. Fuseri, V. Garitey, M. Silvestri, P. Roquebert, and J. Sainsous. Radial force of coronary stents: a comparative analysis. *Catheter Cardiovasc. Interv.* 46:380–391, 1999.
- <sup>45</sup>Rogers, C., and E. R. Edelman. Endovascular stent design dictates experimental restenosis and thrombosis. *Circulation* 91:2995–3001, 1995.
- <sup>46</sup>Rosamond, W., *et al.* Heart Disease and Stroke Statistics—2007 Update, Vol. 115. A Report From the American Heart Association Statistics Committee and Stroke Statistics Subcommittee, 2007.
- <sup>47</sup>Serruys, P. W., P. de Jaegere, F. Kiemeneij, C. Macaya, W. Rutsch, G. Heyndrickx, H. Emanuelsson, J. Marco, V. Legrand, P. Materne, J. Belardi, U. Sijwart, A. Colombo, J. Goy, P. van den Heuvel, J. Delcan, and M. Morel. A comparison of balloon-expandable-stent implantation with balloon angioplasty in patients with coronary artery disease. Benestent Study Group. *N. Engl. J. Med.* 331:489–495, 1994.
- <sup>48</sup>Stadler, M., and G. A. Holzapfel. Subdivision schemes for smooth contact surfaces of arbitrary mesh topology in 3D. *Int. J. Numer. Meth. Eng.* 60:1161–1195, 2004.
- <sup>49</sup>Stadler, M., G. A. Holzapfel, and J. Korelc.  $C^n$ -continuous modeling of smooth contact surfaces using NURBS and applications to 2D problems. *Int. J. Numer. Meth. Eng.* 57:2177–2203, 2003.
- <sup>50</sup>Stone, G. W., S. G. Ellis, D. A. Cox, J. Hermiller, C. O'Shaughnessy, J. T. Mann, M. Turco, R. Caputo, P. Bergin, J. Greenberg, J. J. Popma, M. E. Russell, and TAXUS-IV Investigators. One-year clinical results with the slow-release, polymer-based, paclitaxel-eluting TAXUS stent: the TAXUS-IV trial. *Circulation* 109:1942–1947, 2004.
- <sup>51</sup>Sullivan, T. M., S. D. Ainsworth, E. M. Langan, S. Taylor, B. Snyder, D. Cull, J. Youkey, and M. Laberge. Effect of endovascular stent strut geometry on vascular injury, myointimal hyperplasia, and restenosis. *J. Vasc. Res.* 36:143–149, 2002.
- <sup>52</sup>Taylor, R. L. FEAP—A Finite Element Analysis Program, Version 7.5 User Manual. Berkeley, CA: University of California at Berkeley, 2005.
- <sup>53</sup>Wang, W. Q., D. K. Liang, D. Z. Yang, and M. Qi. Analysis of the transient expansion behavior and design optimization of coronary stents by finite element method. *J. Biomech.* 39:21–32, 2006.
- <sup>54</sup>Xia, Z., F. Ju, and K. Sasaki. A general finite element analysis method for balloon expandable stents based on repeated unit cell (RUC) model. *Finite Elem. Anal. Des.* 43:649–658, 2007.